Vortex Driving Mechanism in Oscillatory Rocket Flows

G. A. Flandro*
Georgia Institute of Technology, Atlanta, Georgia

Several mechanisms that cause hydrodynamic instability of sheared regions of flow in a rocket chamber to drive acoustical oscillations are integrated into a comprehensive model for the vortex shedding phenomenon in this analysis. The energy method is utilized to enable later extension of the linear theory described in this paper to finite amplitude problems in which nonlinear effects are likely to be dominant. A detailed model of the feedback effect that links the acoustical and vortical fields in the vicinity of the shear layer origin is presented. This is a vital element since it provides the phasing and also the strength of the vortical waves relative to the superposed acoustic field. The most important mechanism involved in the transfer of vortical energy into the acoustic field is the interaction of the vortices with a solid surface of impingement at a suitable distance and location downstream from the shear layer origin. The energy transfer in this case is equivalent to a dipole sound source, and a more efficient mechanism than the volume quadrapole effects that have previously been evaluated. Two useful analytical tools emerge. The first is a simple rule by which designers can make the necessary changes in internal ballistics to eliminate or reduce vortex driven oscillations. The second is a growth rate model that allows a quantitative assessment of vortical interactions and is compatible with the standard acoustic stability assessment procedures in widespread use.

Nomenclature

A = linear growth rate
a_0 = speed of sound
C = complex amplitude of vortical wave at shear layer origin
d = impingement surface standoff distance
e_r, e_θ, e_z = unit vectors in radial, circumferential, and axial directions, respectively
E = energy density
$\mathcal{E}_0$ = time averaged linear acoustic energy
f = frequency, Hz
$\mathfrak{F}$ = body force per unit volume
h = width of impingement surface
H = enthalpy function defined by $\nabla H = \nabla P/\rho + \nabla (u \cdot u)/2$
I = acoustic intensity
k = wavenumber
m = mass flux vector
M_0 = mean flow Mach number
M_0 = mean flow velocity vector
p = pressure
r = radial coordinate
R_0 = radial location of critical axis
S = Strouhal number
t = time
u = velocity vector
u' = acoustic velocity perturbation
$\tilde{u}$ = vortical velocity perturbation
U_0 = mean flow velocity
W = axial velocity component
y = local coordinate normal to mean flow vector
z = axial coordinate (z' is axial distance from acoustic pressure node)
Z_0 = location of point of separation relative to acoustic pressure node
α = temporal growth rate
$\alpha_r + i\alpha_i$ = complex vortical eigenvalue
γ = ratio of specific heats
Γ = production of acoustic energy per unit volume
δ = momentum thickness of shear layer
ϵ = amplitude of fluctuations
ρ = density
ω = circular frequency (dimensionless)
Ω = mean vorticity vector
ζ = oscillatory vorticity
Ψ' = stream function
ξ = amplitude of oscillatory vorticity
ϕ = amplititude of stream function
$< >$ = time average of enclosed function

Superscripts

$( )'$ = time-dependent function
$(\tilde{})$ = vortical fluctuation

Subscript

$( )_0$ = denotes reference value

Received Oct. 1, 1985; revision received Nov. 25, 1985.

*Professor of Aerospace Engineering. Associate Fellow AIAA.

Introduction

EXTENSIVE cold flow experimentation[1] and full-scale motor testing[2] have verified that vortex shedding is one of several mechanisms that drive pressure oscillations in rockets as first suggested by Flandro and Jacobs.[3] Although vortex driven sound has been studied extensively in other contexts for many decades,[4,5] no theories have been forthcoming that are useful in the practical system analysis of rocket motors and ramjets. Models of the vortex shedding process are therefore needed, and these models must be configured to be compatible with the accepted representations of pressure oscillations from other sources, such as pressure-coupled combustion. It is necessary to recognize the multiplicity of paths of energy flow between vortical oscillations produced in separated regions of gas flow and the standing acoustic waves in the chamber. Also, the geometrical complexities of actual combustion chambers must be addressed. All of these considerations set the goals for the present analysis. In addition to providing means for incorporating vortex shedding effects directly in standard linearized acoustic instability models, the analysis presented herein yields design procedures that allow the rocket motor designer to avoid vortex driven oscillations by appropriate attention to the motor grain geometry and internal ballistics.

Figure 1 shows a typical flow pattern and port geometry combination that is known to have generated vortex driven oscillations in solid propellant motors.[2] The large forward burning surface area produces a mass flow contribution which does not merge smoothly with the combustion products emerging from the centerbore. A sheared flow is produced, as shown in Fig. 1, and the shear strength is enhanced by the "doughnut" constriction at the centerbore/slot transition. If the velocity gradient is sufficiently large, then this shear layer is unstable and small disturbances in the vicinity of the origin are amplified spatially forming large scale periodic vortex ring structures. These vortices translate in the direction of and at a speed generally lower than the local mean flow. There is an initial region of linear spatial growth followed by a zone of complex nonlinear interactions in which dispersal, decay, and vortex pairing may take place. Degradation of vortex structures is inhibited in the presence of an organizing signal such as a superimposed sound field. Decay is also delayed in the presence of the favorable pressure gradient that is a natural feature of a rocket motor flowfield.

Energy passes from the vortex fluctuations to the acoustic field in a variety of ways. The important dipole mechanism involves the interaction of the vortices with an impingement surface located near the critical axis.† The distance between the point of separation and the point of impingement, referred to in this paper as the "standoff distance," must be of the order of the vortical wavelength. The energy transfer is critically dependent on the spacing, since it affects the phasing of the pressure impulse generated at the impingement point relative to the acoustic wave structure. A useful conceptual model is based on the idea that associated with the vortical wave motions produced by the hydrodynamic instability is a pseudosound pressure field. This pressure disturbance propagates with the large scale vortical structures at some fraction of the local mean flow velocity in the downstream direction. These oscillations are confined to the relatively compact region of the vortical disturbance; they do not propagate as sound waves and, therefore, do not interact directly with acoustic waves in the surrounding chamber, except in the manner of quadrapole excitation represented by the vortex wave undulations. However, when vortical waves interact with a solid surface of impingement, oscillating hydrodynamic forces are generated and an important sound source may be produced. Much past effort has been devoted to the linking of these forces to the effective dipole strength of the sound source.[5-7] Most models of this sort are of limited use in the present context for the following reasons: 1) they are aimed at determining far field radiation effects in an unbounded region of flow; 2) geometrical features that are peculiar to the rocket motor application are not represented; and 3) oversimplified representations of the vortices are assumed. Much of the present paper is devoted to eliminating these deficiencies.

Figure 2 shows in diagrammatic form the elements necessary for a self-consistent predictive model for vortex generated sound in a rocket combustion chamber. Of central importance is the hydrodynamic stability model. Several extensions of the theory were carried out in the course of this study, including accommodation of arbitrary shear layer profiles and nonlinear spatial growth effects. A pivotal element is the correct modeling of the coupling feedback effect that provides the signal that is amplified in the shear layer. Since previous theory is rather vague in this regard, it was necessary to establish the details of the mechanisms involved as part of the present effort. Both of the quadrapole and dipole mechanisms of energy transfer from the vortical fluctuations into the acoustic field are assessed.

†The critical axis is defined as a coordinate axis everywhere parallel to the local mean flow velocity vector with its origin at the axial location of the point of separation and the radial location of the point of maximum mean flow radial velocity gradient. This axis forms the basic coordinate system for analysis of shear layer instability.

Formulation

Reviewed in this section are the assumptions and physical bases upon which the complete system analysis is constructed. Since two oscillatory components are involved, it is essential that appropriate sets of variables be defined for each component with the necessary linkages between the two sets. Two major flow domains with quite different characteristics must be addressed. The first is the compressible chamber mean flow with a superposed acoustic wave structure. Embedded within this flow is a region which is dominated by rotational effects that will be referred to as the vortical or "hydrodynamic" region. Table 1 defines a set of definitions that is compatible with the requirements of a useful coupled vortical/acoustical system. Both hydrodynamic and acoustic flow domains utilize the same time scale since the feedback from the acoustic wave provides the controlling signal for the hydrodynamic instability. Taken alone, the vortical disturbances are disorganized and ultimately contribute to chamber turbulence. In the presence of an acoustic wave in the correct frequency range, a strong correlative signal is present which organizes the vortical disturbance, sets its phase relative to the acoustic system, and provides the initial fluctuation level that is amplified spatially in the downstream direction. This "locking-in" phenomenon is often observed experimentally[8] and characterizes most situations in which finite vortical disturbances appear.

Two perturbation parameters will be exploited. ϵ is the amplitude of the acoustic wave system and M_0 is the mean flow Mach number defined at the origin of the sheared flow critical axis. The latter is conveniently referenced to the Mach number of the mean flowfield at the axial station corresponding to the shear layer origin. It is assumed that both parameters are small compared to unity. Since compatibility with existing rocket acoustic instability analyses is desired, terms are retained to first order in ϵ; only linear terms in mean flow Mach number need be retained.

The following assumptions are utilized: 1) irrotational acoustic oscillation, 2) incompressible vortical oscillations, 3) inviscid perfect gas, and 4) isentropic flow in the acoustic

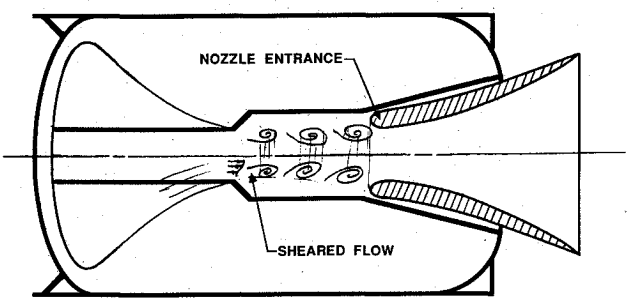

Fig. 1 Vortex generation in sheared zone at slot/centerbore transition.

Table 1 Dimensionless variables

	Acoustical	Vortical
Position	$r=r^a/L$	$r=r^a/\delta$
Velocity	$u'=u^a/ao$	$u=u^a/Wo$
Time	$t=(ao/L)t^a$	$t=(ao/L)t^a$

Note: ao = speed of sound; L = chamber characteristic length; Wo = maximum mean flow velocity at separation point; δ = shear layer momentum thickness; S = Strouhal number $=(\delta/Wo)/(L/ao)\ \omega$; and the pressure is normalized by γPo, density by ρo, and temperature by To. [a]Dimensional variable.

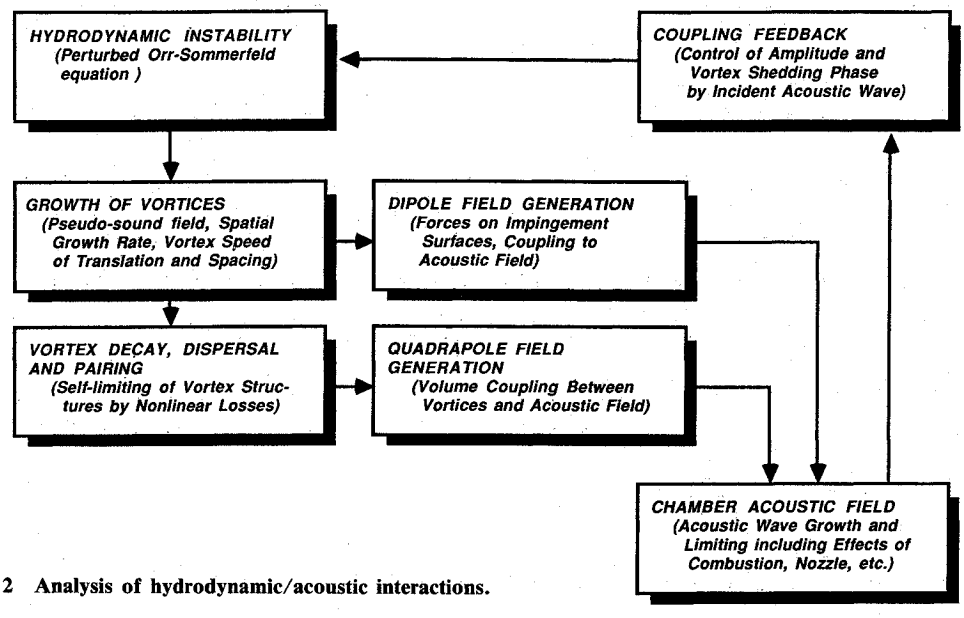

Fig. 2 Analysis of hydrodynamic/acoustic interactions.

domain. The first and second assumptions are equivalent to the "splitting theorem" that ascribes solenoidal characteristics to the vortical components and irrotational attributes to the acoustic motions.

Using the dimensionless variables defined in Table 1, the governing continuity and momentum equations are:

Acoustical:

$$\partial\rho/\partial t+\nabla\cdot(\rho u)=0 \tag{1}$$

$$\rho Du/Dt=-\nabla P+\mathfrak{F} \tag{2}$$

Vortical:

$$\nabla\cdot u=0 \tag{3}$$

$$\partial/\partial t(\nabla\times u)-\nabla\times(u\times\nabla\times u)(\omega/S)=\nabla\times\mathfrak{F}/M_0 \tag{4}$$

$\mathfrak{F}$ is the body force vector acting (per unit volume) on a given element of gas. The vortical momentum equation is written in vorticity form for later convenience. The scaling factor S in the vortical momentum equation is the Strouhal number defined as

$$S=\omega(\delta/L)/(U_0/a_0) \tag{5}$$

δ is assumed to be small compared to the acoustic wavelength which in turn is taken to be of the order of the chamber characteristic length L. The value of S determines the response of the shear layer to the acoustic perturbations. Amplification occurs only within a certain Strouhal number range, a result that follows directly from the vortical domain solutions and reflects a large body of experimental evidence.

Vortical/Acoustical Energy Balance

The energy method simplifies the analysis of coupled hydrodynamic/acoustic interactions, and provides a foundation on which to build nonlinear models. The rate of change of energy density E is governed by a relationship of the form

$$dE/dt=-\nabla\cdot I+\Gamma \tag{6}$$

If the gas is assumed to be calorically perfect, the continuity and momentum equations for the acoustic field [Eqs. (1) and (2)] can be written as

$$\partial\rho/\partial t=-\nabla\cdot m \tag{7}$$

$$\partial u/\partial t=-\nabla H+(u\times\nabla\times u)+\mathfrak{F}/\rho \tag{8}$$

All variables are comprised of slowly varying and rapidly oscillating components such that

$$P=1/\gamma+p' \tag{9}$$

$$\rho=1+\rho' \tag{10}$$

$$u=M_0+u' \tag{11}$$

and so on for the other variables. The rapidly oscillating components are taken to be composed of periodic functions with amplitudes that may change slowly compared to the period of the oscillations. Taking ϵ to be the instantaneous amplitude of the fluctuations, the primary variables are conveniently expanded in the form

$$H'=\epsilon H_1+\epsilon^2H_2+\mathcal{O}(\epsilon^3)$$

$$m'=\epsilon m_1+\epsilon^2m_2+\mathcal{O}(\epsilon^3)$$

$$\rho'=\epsilon p'+\epsilon^2p'^2(1-\gamma)/2+\mathcal{O}(\epsilon^3) \tag{12}$$

where primes denote the fluctuating part of the variable. Expansion of the enthalpy function yields a set of terms of the form

$$H_1=p'+M_0\cdot u'$$

$$H_2=(p'^2+u'\cdot u')/2 \tag{13}$$

The mass flux to various orders is

$$m_1=u'+M_0p'$$

$$m_2=p'u'+M_0(1-\gamma)p'^2/2 \tag{14}$$

and so on. For brevity, only functions required in evaluating the linear growth rate will be displayed. The full machinery needed for dealing with the nonlinear problem to any order in ϵ is described in Ref. 9 using a slightly different format.

The energy density E is also a nonlinear function of wave amplitude; thus E', the fluctuating part of acoustic energy density, is expanded as

$$E'=\epsilon^2E_1+\epsilon^3E_2+\ldots \tag{15}$$

The series begins with a term proportional to ϵ^2 since the linear acoustic energy is a quadratic combination of the primary time-dependent variables. The leading term is

$$E_1 = p'^2/2 + M_0 \cdot u' p' + u'^2/2 \tag{16}$$

Multiplication of the continuity equation [Eq. (7)] by H' and combining with the scalar product of the momentum equation [Eq. (8)] with m' yields the required energy balance relationship

$$\partial E'/\partial t = -\nabla \cdot (H' m') + m' \cdot (u \times \nabla \times u + \mathcal{F}/\rho) \tag{17}$$

where $\Gamma = m' \cdot (u \times \nabla \times u + \mathcal{F}/\rho)$ is the energy production. The production term represents both effects of vorticity transport in rotational regions of the flowfield and dipole effects due to interaction of vortices with immersed bodies or boundaries. Vector u in vorticity terms is the sum of the mean and oscillatory velocity; both mean and fluctuating vorticity must be accounted for. Source effects due to combustion within the volume are neglected. Viscous and thermal nonuniformity are assumed to be confined to thin regions near the burning surface. Volume nonisentropic losses, such as those arising in steep-fronted waves, are assumed to arise in regions of negligible thickness that can be treated as discontinuities.

Taking the time average of Eq. (17) and integrating over the chamber volume yields the rate of change of the system oscillatory energy,

$$\partial/\partial t [\epsilon^2 \Gamma_1 + \epsilon^3 \mathcal{E}_2 + \epsilon^4 \mathcal{E}_3 + \ldots] = -\int_V \langle \nabla \cdot (H' m') + \Gamma \rangle dV \tag{18}$$

where

$$\mathcal{E}_n = \int_V \langle E_n \rangle dV$$

is the time-averaged system energy of order n. The slow (relative to the oscillations) rate of change of system amplitude finally takes the form

$$d\epsilon/dt = \epsilon A + \epsilon^2 B + \epsilon^3 C + O(\epsilon^4) \tag{19}$$

The functions A, B, and C are expressions involving volume and surface integrals over the chamber domain.[9] For the present purposes, only the linear function A is of interest. A is equivalent to the well-known linear growth rate, but has been extended to include the vortical driving effects. The linear behavior is governed by

$$A = \alpha = -(\tfrac{1}{2}\mathcal{E}_0)\left[\int_S \langle n \cdot [p' u' + (M_0 \cdot u') u' + M_0 p'^2] \rangle dS - \int_V \langle m' \cdot (u \times \nabla \times u + \mathcal{F}/\rho) \rangle dV\right] \tag{20}$$

where $\mathcal{E}_0$ is the classical time averaged linear acoustic energy

$$\epsilon_0 = \int_V \langle p'^2/2 + u' \cdot u'/2 \rangle dV \tag{21}$$

The growth rate expressions will be evaluated in detail after the vortex shedding model and the representation of interaction of vortices with impingement surfaces have been completed.

Modeling of Hydrodynamic Instability

As a major component in the evaluation of the acoustic stability integrals, a comprehensive model of the vortical oscillations and their coupling to the acoustic field must be constructed. Attention is now focused on Eqs. (3) and (4) which are scaled properly for the vortical region of flow. The velocity at any point in this region may be represented as the superposition of three components: 1) the sheared mean flow, 2) the acoustic velocity, and 3) the hydrodynamic time-dependent velocity field. Thus, in the dimensionless variables of the vortical region,

$$u = U_0 + u'/M_0 + \tilde{u} \tag{22}$$

where the acoustic component has been left in the same form as used in the acoustical region to simplify its inclusion in the vortical feedback process. The vorticity is governed by

$$(S/\omega)(\partial \zeta/\partial t) = \nabla \times (U_0 \times \zeta) + \nabla \times (\tilde{u} \times \Omega) + \nabla \times (u' \times \Omega)/M_0 \tag{23}$$

where S is the Strouhal number, $U_0 = U e_r + W e_z$ is the mean flow velocity, Ω is the mean vorticity vector ($\nabla \times U_0$), and ζ is the oscillatory vorticity ($\nabla \times \tilde{u}$). The last term on the right represents the acoustic interaction with the vortical field. Consideration of this term leads to a major improvement in correspondence between theory and experiment. It sets the phase and amplitude of the vortical waves and thus provides the much-discussed and observed feedback effect which channels the hydrodynamic motions into a narrow band oscillation. Since Eq. (23) is linear, it is solved by first determining the complementary function with the feedback term suppressed. Account of the feedback is taken in the form of the particular integral of Eq. (23), and the complete solution is then adjusted to satisfy appropriate boundary conditions. In this manner, the main link between vortical and acoustical oscillations is forged, and identification of the vortical sound sources is implemented. Equation (3) is satisfied by introducing the streamfunction Ψ such that

$$u = -(1/r)\partial \Psi/\partial z \quad \text{and} \quad w = (1/r)\partial \Psi/\partial r \tag{24}$$

A spatially growing, axisymmetric, harmonic wave motion is to be modeled. Thus, it is appropriate to put

$$\Psi = C\phi(r)\exp[i(\alpha z - \omega t)]$$
$$\zeta = C\xi(r)\exp[i(\alpha z - \omega t)]e_\theta \tag{25}$$

where C is an amplitude constant (complex) which must satisfy the boundary conditions at the shear layer origin. Since the vorticity and the stream function are related by

$$|\zeta| = -(1/r)[\partial^2 \Psi/\partial z^2 + \partial^2 \Psi/\partial r^2 - (1/r)\partial \Psi/\partial r]$$

then

$$\xi(r) = (1/r)[\alpha^2 \phi - \partial^2 \phi/\partial r^2 + (1/r)\partial \phi/\partial r] \tag{26}$$

Using Eq. (26) to write (24) in terms of the complex complementary function ϕ, the axisymmetric form for the Rayleigh hydrodynamic stability equation is found:

$$[\partial W/\partial z + i(\alpha W - S)][\alpha^2 \phi - \partial^2 \phi/\partial r^2 + (1/r)\partial \phi/\partial r] - (\partial^2 W/\partial r \partial z)\partial \phi/\partial r + i\alpha[\partial^2 W/\partial r^2 - (1/r)\partial W/\partial r]\phi = 0 \tag{27}$$

This equation must be solved for ϕ and the eigenvalue $\alpha = \alpha_r + i\alpha_i$ by numerical means, since the variable coefficients are complicated functions of the spatial variables. Flandro and Finlayson[10] have determined solutions for arbitrary mean flow profiles. Michalke[11] studied solutions for the planar case based on the useful hyperbolic tangent representation for the mean flow velocity profile.

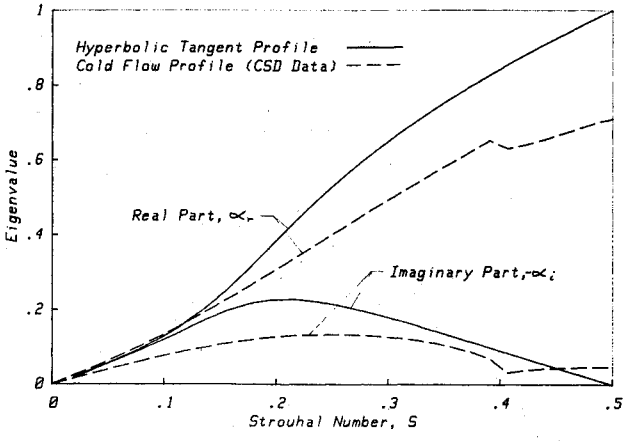

Fig. 3 Shear instability eigenvalue vs Strouhal number.

Freymuth[12] verified these solutions experimentally. The axisymmetric solution is identical to the planar one if the radial location of the sheared flow is large compared to the momentum thickness of the shear layer. All results presented herein correspond to this case.

The imaginary part of the α, α_i represents the spatial growth rate. An important feature of the solution is that the imaginary part of the eigenvalue is nonzero only over a limited Strouhal number range between $0<S<S_{max}$. The value of S that corresponds to maximum, spatial amplification is approximately 0.2 and S_{max} is 0.5 for the hyperbolic tangent profile. Low values of Strouhal number are favored because S is proportional to the thickness of the sheared zone, and an intense shear is indicated by small values of the momentum thickness. Figure 3 is a plot of the real and imaginary parts of α vs the Strouhal number S. The solid curves are the results for the hyperbolic tangent velocity profile (Fig. 4a); the dashed curves show the behavior for the velocity profile illustrated in Fig. 4b. This profile represents actual shear layer velocity data obtained in a recent cold flow simulation[1] plotted vs $y=(R_0-r)$. R_0 is the radial location of the critical surface as illustrated in Fig. 5. The left-hand parts of Fig. 4a and 4b show the physical data; the right-hand parts show the profile in the transformed coordinate $y_h=\tanh(R_0-r)$. This clearly indicates the deviation of the data from the hyperbolic tangent reference profile, since the latter plots as a straight line in the transformed plane.

The velocity profile shape affects in an important way both the vortical wavelength ($2\pi\delta/\alpha_r$) and the spatial growth rate α_i as shown in Fig. 3. The measured profile exhibits considerably lower values of spatial growth over the important part of the Strouhal number range. This indicates the importance of representing realistic shear layer profiles in numerical calculations. The results indicate that for the velocity profile of Fig. 4b, the Strouhal number range over which vortical instability is possible is somewhat wider than for the hyperbolic tangent profile, but has a very low spatial growth rate in the extended region.

Figure 6 shows the hyperbolic tangent eigenvector ϕ plotted vs y for $S=0.2$. Figure 7 is a similar plot for the velocity profile of Fig. 4. It will be noticed that the shape of the vortical fluctuation as represented by ϕ is strongly affected by the velocity distribution in the shear layer. Since knowledge of the vortex geometry is required in any estimates of energy flux to the acoustic field, it is again essential to treat realistic velocity profiles in the numerical calculations.

Since the coupling of the vortical fluctuations to the superposed sound field is the ultimate goal, it is necessary to establish the phase and amplitude of the vortical waves relative to the acoustic waves. This is accomplished by determining the particular integral of Eq. (23) which accounts for the presence of the acoustic field. The complete vortical solution must then satisfy an appropriate boundary condition which yields the necessary information on the vortex wave phase and amplitude. The particular solution must satisfy

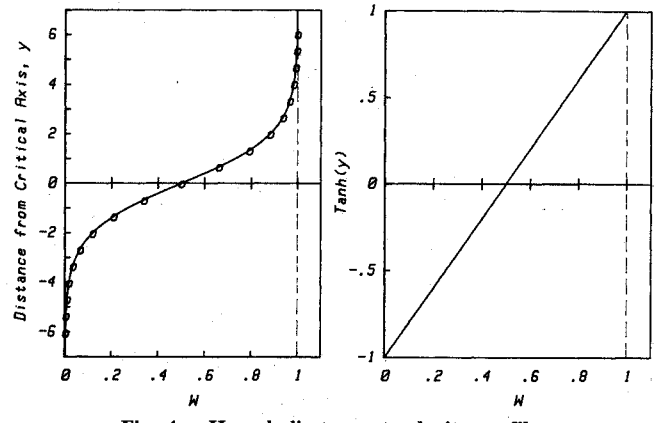

Fig. 4a Hyperbolic tangent velocity profile.

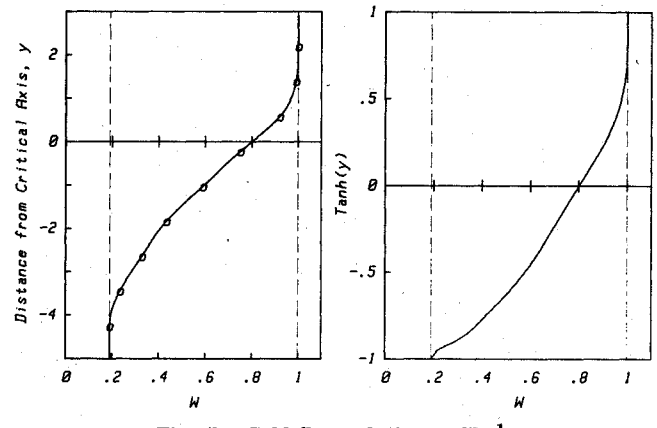

Fig. 4b Cold flow velocity profile.[1]

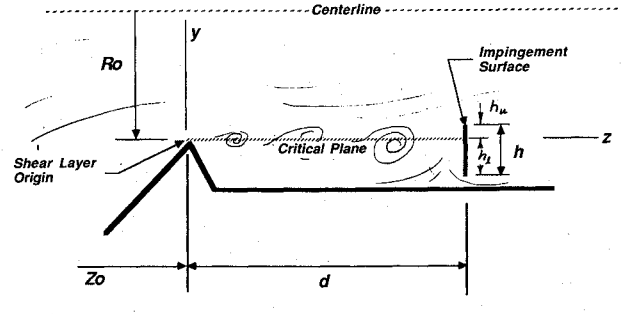

Fig. 5 Geometry of shear layer and impingement surface.

$$\partial\zeta_p/\partial t-(\omega/S)\nabla\times[U_0\times\zeta_p+\tilde{u}_p\times\Omega]$$
$$=(\omega/M_0S)\nabla\times(u'\times\Omega) \tag{28}$$

Assuming a longitudinal acoustic wave, it is appropriate to assume

$$u'=-i\sin(kz')\exp(-i\omega t)e_z \tag{29}$$

z' represents position relative to the forward end of the chamber. Since the origin of the coordinate system used in the vortex shedding analysis is at the shear layer origin located at position Z_0 in z' coordinates, it is necessary to apply the transformation $z'=Z_0+(\delta/L)z$ where z is the axial location as expressed in vortical units. Thus, the nonhomogeneous term becomes

$$(\omega/M_0S)\nabla\times(u'\times\Omega)$$
$$=ik\Omega\exp(-i\omega t)\cos[kZ_0+k(\delta/L)z] \tag{30}$$

The expressions within the square brackets on the left side of Eq. (28) are of the order of M_0 and are, thus, an order of magnitude smaller than the terms eventually retained. Therefore, it is appropriate to set

$$\zeta_p = \xi_p(r)\exp(-i\omega t)\cos[kZ_0 + k(\delta/L)z] \tag{31}$$

and the magnitude of the mean shear layer vorticity is

$$\xi_p(r) = -\Omega(r) \tag{32}$$

The boundary condition that must be satisfied by the complete solution of the vortex wave equation is that the initial value of the composite time-dependent vorticity is zero at the origin of the shear layer where vortical oscillations begin. It is necessary that

$$\zeta \neq \zeta_c + \zeta_p = 0 \text{ at } r = R_0 \text{ and } z = 0 \tag{33}$$

Therefore, the value of the shear wave vorticity at the origin is established. The result is

$$C\xi(R_0) = \Omega(R_0)\cos(kZ_0) \tag{34}$$

There is a strong dependence on the positioning of the shear layer origin relative to the acoustic wave structure and on the strength of the shear stress in the mean flow. Since vortical velocity distributions are required in the stability calculations, Eq. (34) must be used to establish the amplitude of the stream function ϕ. This is accomplished by solving Eq. (34) for the amplitude/phase factor C and using Eq. (26) to write

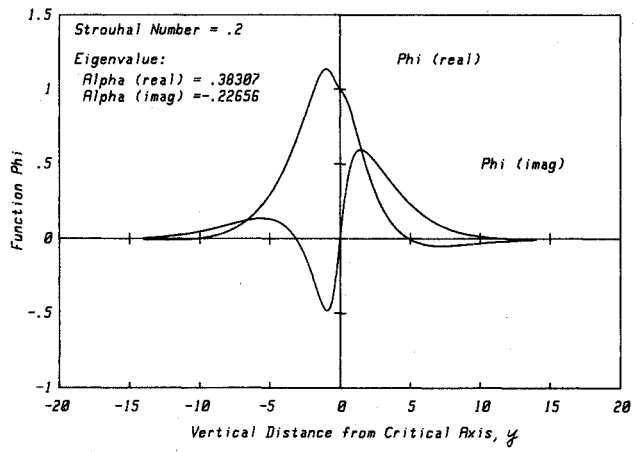

Fig. 6 Eigenfunction vs y for hyperbolic tangent profile.

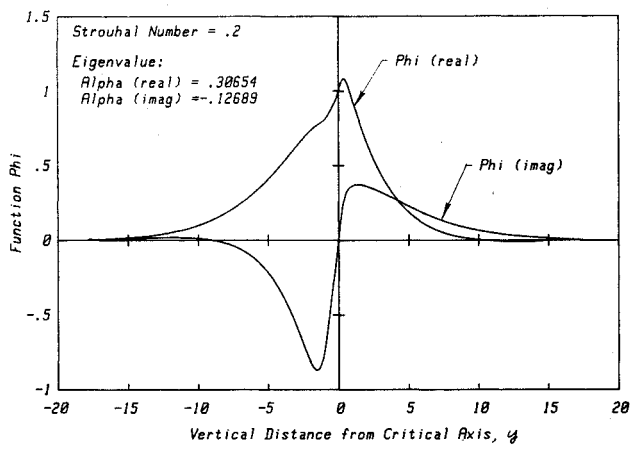

Fig. 7 Eigenfunction vs y for cold flow velocity profile.

$\xi(R_0)$ in terms of the known function ϕ. The result is

$$C = C_r + iC_i = [R_0^2\cos(kZ_0)/(\alpha_r^2 + \alpha_i^2)]$$
$$\times\{[W(R_0)(\alpha_r^2 + \alpha_i^2) - \alpha_r S] + i[\alpha_i S]\} \tag{35}$$

where $W(R_0)$ is the axial shear flow velocity at the origin. Figure 8 shows plots of C_r and C_i for the hyperbolic tangent velocity profile as solid lines, and results for the cold flow data are superimposed for comparison. The differences reflect the sensitivity to details of the velocity distribution already mentioned. The time-dependent vortical velocity components at any downstream point are found from the stream function in final form:

$$\Psi = [(C_r\phi_r - C_i\phi_i) + i(C_i\phi_r + C_r\phi_i)]\exp[i(\alpha z - \omega t)] \tag{36}$$

All necessary shear wave information is now available and evaluation of the system stability integrals can be carried out.

Linear Theory of Vortically Driven Acoustic Waves

In this section, the acoustic growth rate integrals which summarize the effects of vortical fluctuations on the acoustic field to first order in the wave amplitude are evaluated. First, the quadrapole effects represented by the first term in the volume integral in Eq. (20) are assessed. Then the dipole driving represented by the force $\mathfrak{F}$ is evaluated. The latter will be demonstrated to be the dominant form of acoustic wave excitation by vortex shedding in rocket motor applications. This result is verified by experiment, and vortex impingement surfaces have been involved in every experimental arrangement known to the author in which finite amplitude vortex driven sound was observed.

The acoustic growth contribution due to volume quadrapole interactions and related effects is governed by

$$\alpha_q = -(M_0/2\mathcal{E}_0)\int_V \langle (\boldsymbol{u}' + M_0\boldsymbol{p}')\cdot(M_0$$
$$\times\boldsymbol{\zeta} + \boldsymbol{u}'\times\boldsymbol{\Omega} + M_0\tilde{\boldsymbol{u}}\times\boldsymbol{\Omega})\rangle \mathrm{d}V \tag{37}$$

to appropriate order in wave amplitude. Of the six components of the expanded integrand in Eq. (37), only one is linear in M_0. The other five, including the classical quadrapole terms, are neglected since they are of the order of M_0^2. The resulting theory is compatible with the standard combustion instability assessment techniques, and is based on the assumption that the mean flow Mach number is small everywhere in the chamber. Thus, terms which are the traditional sources of quadrapole driving are neglected in comparison to

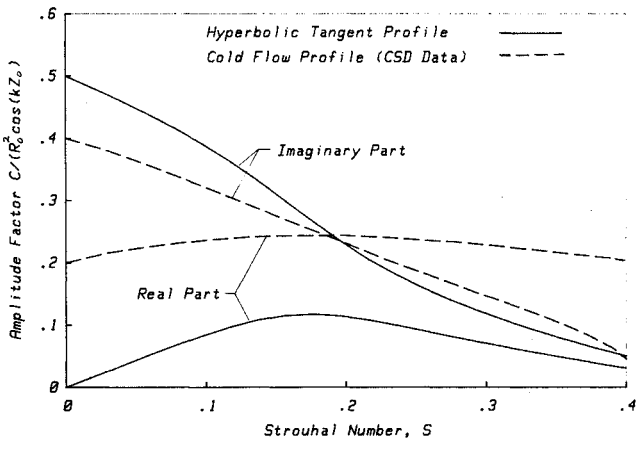

Fig. 8 Vorticity amplitude function vs Strouhal number.

more efficient sources of acoustic energy, such as pressure coupling with the burning surface. To the required order in mean flow Mach number, the expression

$$\alpha_q = -(M_0/2\mathcal{E}_0)\int_V \langle u' \cdot (u' \times \Omega)\rangle dV + \mathcal{O}(M_0^2) \quad (38)$$

gives the influence of this set of terms. In the present case, interest is focused on the intense mean flow vorticity Ω concentrated near the critical plane. As a consequence of the geometry and assumption of axial acoustic modes, Eq. (38) yields a zero growth rate increment. Situations undoubtedly exist in which this would not be true. However, the result is proportional to the volume of the vortex shedding region; therefore, α_q is proportional to δ, the shear layer momentum thickness. For cases of interest, this is a small factor, and, thus, for practical situations, the contribution from α_q is, most likely not large. Interactions similar to these have been discussed previously by Culick.[13] He deduced the growth rate corrections due to the influence of a rotational mean flowfield filling the chamber; no further assessment is required here. Also, the surface integral terms of Eq. (20) are the basis for the classical combustion instability theory and will receive no further attention in this paper.

Of greater interest than the volume interactions are the dipole effects which are represented symbolically in terms of the force $\mathcal{F}$ in Eq. (20). Determination of this force, which represents the interaction of the vortical field with a downstream impingement surface, is one of the truly challenging problems in the analysis. Indeed, this is the point at which most analyses end. One must determine the time-dependent surface force distribution on a boundary (of arbitrary shape and orientation relative to the stream) caused by interaction with the complex flow with embedded large scale structures. It is possible to determine the force explicitly by means of appropriate finite element calculations, but a reliable algorithm which is not severely geometry dependent has not yet emerged. It is thus appropriate to employ approximations which are compatible with those already used in the other elements of the analysis. This is accomplished by using the fact that a rigid boundary acted upon by a pressure distribution can be represented by the body force

$$\mathcal{F} = p\delta(n)e_n \quad (39)$$

where p is the pseudosound pressure distribution resulting from the vortex shedding, $\delta(n)$ the Dirac delta function in terms of the normal coordinate n measured from the boundary, and e_n the unit normal vector to the boundary at the point in question. It is first necessary to develop an expression for the pseudosound field to be used with Eq. (39) for integration in Eq. (20). This can be readily accomplished for simple geometrical situations.

The vortical pressure fluctuation or "pseudosound" oscillation is found directly in terms of the vortical domain velocity field by means of the momentum equation. The gradient of the pseudosound pressure distribution is

$$\nabla p = M_0[-\partial u/\partial t - \nabla(U_0 \cdot \tilde{u}) + U_0 \times \zeta + \tilde{u} \times \Omega] + u' \times \Omega \quad (40)$$

where the scale is adjusted to the acoustical domain for use in Eq. (20). This is easily integrated with the result

$$p = M_0 C/R_0[\partial\phi/\partial r(\omega S/\alpha - W) + \phi(\partial W/\partial r)]\exp[i(\alpha z - \omega t)] \quad (41)$$

where the notation is identical to that used in the last section. The result is expressed in terms of the vortical streamfunction $\phi(r)$ for convenience. This represents a spatially growing pressure oscillating not to be confused with the acoustic pressure fluctuations, since it does not propagate in the same manner and is tied to the volume occupied by the vortex structures. Knowledge of this pressure distribution enables the estimation of the oscillation force on the impingement surfaces. This is accomplished using Eq. (39) and assuming the vortical domain is compact compared to the chamber characteristic size. Finally, insertion of this representation for the force into Eq. (20) using Eq. (14) for the mass flow rate gives the expression for the linear growth rate contribution due to surface dipole interaction with the vortical structures. The result to appropriate precision is

$$\alpha_d = \left(\frac{1}{2}\mathcal{E}_0\right)\int_V \langle u' \cdot p\delta(n)e_n\rangle dV \quad (42)$$

Due to the presence of the delta function, the volume integration reduces to surface integration over area elements perpendicular to e_n. It must be noted that this unit vector points *into* the chamber from the surface element representing the direction of the force *on* the fluid in the acoustical domain exerted by the hydrodynamic pressure oscillations felt by the surface.

To illustrate the manner in which Eq. (42) is evaluated, a simple example is presented that represents one interpretation of the driving mechanism at work in the geometry of Figure 5. The impingement surface is taken to be normal to the chamber axis and also to the local mean flow direction. Interpreting Eq. (42) as described, the growth rate is found to be

$$\alpha_d = 2n\pi(R_0/R)^2 f(Z_0,d)g(S,d) \quad (43)$$

where R_0/R is the ratio of the radial position of the critical plane to the chamber radius, and n is the mode integer. Function f is the main geometrical factor. For the assumed longitudinal acoustic mode of oscillation it is

$$f(Z_0,d) = \cos kZ_0 \sin k(Z_0 - d) \quad (44)$$

where Z_0 locates the origin of the shear layer with respect to the forward end of the chamber as shown in Fig. 5. d is the standoff distance which locates the impingement surface relative to the shear layer origin. Figure 9 is a plot of function f vs Z_0 for several modes and a typical value for the standoff distance ($d = .05$ in acoustic field length units). It is immediately apparent that placement of the shear layer origin *exactly* at the chamber midpoint totally eliminates driving from the dipole mechanism for odd modes. However, strong first and third mode interactions are possible if the separation point is upstream of the chamber midpoint by a small fraction of the chamber length. Notice that at this location, the second mode is severely damped as indicated by a large negative value of f. This would account for the observations of Dunlap and Brown[14] in which a pair of ring baffles were placed in a choked cylindrical chamber straddling the midpoint. First and third acoustic modes were strongly excited while the second mode was not.

The second growth rate factor g is mainly a function of the Strouhal number and the standoff distance d. It also depends on the width h of the impingement surface and its radial placement relative to the critical axis. Again, Fig. 5 describes the geometry. g is expressed in integral form as

$$g(S,d) = [\exp(-\alpha_i d)/S]\int_{h_\ell}^{h_u} \times [-(A_1 - \Omega(0)A_3)\sin\alpha_r d + (A_2 - \Omega(0)A_4)\cos\alpha_r d]\, dr \quad (45)$$

where $\Omega(0)$ is the mean flow shear stress $-\partial W/\partial r$ evaluated at the shear origin and at the critical radius. Its appearance here shows the strong effect played by the shear strength on the vortex driving effect. d is the standoff distance expressed

in vortical domain units; that is, d is normalized with respect to shear layer momentum thickness as it appears in this formula; it is a fraction of chamber radius in the acoustic domain as in Eq. (44). Functions A_n are defined as follows:

$$A_1 = -(D_r^2 - D_i^2)\partial\phi_r/\partial r + 2D_rD_i\partial\phi_i/\partial r$$

$$A_2 = -(D_r^2 - D_i^2)\partial\phi_i/\partial r - 2D_rD_i\partial\phi_r/\partial r$$

$$A_3 = D_r\phi_r - D_i\phi_i$$

$$A_4 = D_r\phi_i + D_i\phi_r \tag{46}$$

The integrals are performed numerically by utilizing the eigenfunction algorithm described earlier which computes the radial dependence of the stream function $\phi(r) = c_r(r) + i\phi_i(r)$. Function D is related to the amplitude/phase function C by

$$D = D_r + iD_i = C/[R_0^2\cos(kZ_0)] \tag{47}$$

Figure 10 shows the sensitivity of function $g(S,d)$ to the standoff distance for several values of the Strouhal number over the range of interest. The results shown are for a surface width h of three times the momentum thickness placed symmetrically at the critical axis. The values of function g are sensitive to width and placement of the impingement surface, a result which is often seen experimentally.

For a positive acoustic growth rate, both functions f and g must have the same sign. The largest contribution to acoustic instability occurs for small Strouhal number, fairly large standoff distance, with the shear origin near the center of the chamber. In some situations, the Strouhal number is closer to the upper cutoff value of approximately 0.5, in which case a larger growth rate results if the standoff distance is small. The g function oscillates as d changes; this corresponds to well-known experiments[5,7] that demonstrate the great sensitivity of the sound production to the standoff spacing. The recent cold flow similations by Dunlap[1] emphasize this observation. Placement of the nozzle entrance (which represents the impingement surface) was shown to have large influence on the measured sound intensity. The observed sensitivity to changes in Strouhal number also corresponds to the predictions given here. Insertion of the geometrical and flow parameters from the experiments described in Ref. 1 results in a positive acoustic growth rate of significant amplitude.

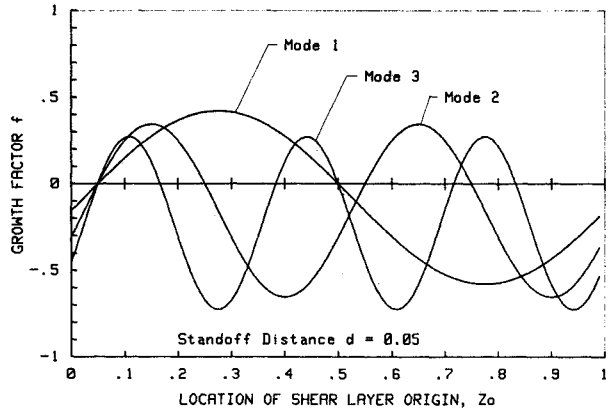

Fig. 9 Growth rate function f dependence on shear layer origin.

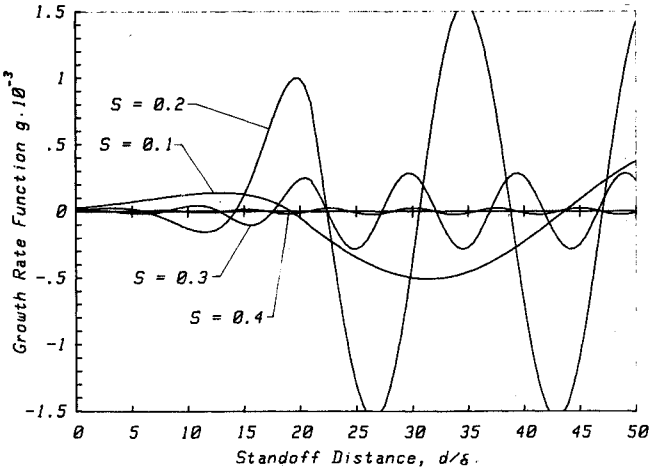

Fig. 10 Growth rate function g vs standoff distance.

In addition to the detailed representation of the acoustical/vortical interactions described in the stability calculations, an important design rule for avoidance of vortex generated pressure oscillations results from the linear theory. General rules based on geometry changes are difficult to formulate since such complex relationships are involved accompanied by a myriad of combinations of the several parameters involved. Also, since motor chamber geometry generally changes significantly during operation, it is almost impossible in practice to be sure that there is not some combination of geometrical factors at some time in the burn that could lead to vortex-driven oscillations if the Strouhal number is in the critical range. The latter observation leads directly to the proposed design rule. The vortex shedding phenomenon itself represents a broadband amplifier of acoustic disturbances, but only over a limited frequency range. It is clear from the analysis presented here that no interaction can occur if the Strouhal number S is greater than approximately 0.5 (accounting for dependence on shear layer velocity distribution, etc.). Assuming a simple longitudinal acoustic wave, it is evident that if

$$S = 2\pi f(\delta/U_0) > 0.5 \tag{48}$$

then no vortical driving occurs. Thus, to avoid vortex shedding effects, it is necessary only that the shear layer momentum thickness near the origin of the sheared region of mean flow must satisfy the inequality

$$\delta > U_0/(4\pi f) \tag{49}$$

where f is the frequency of the mode in question and U_0 is the maximum flow speed at the origin. Thus, in a new motor program, the designer should insure that no sheared regions have momentum thickness smaller than that given in Eq. (49) for any potential mode of oscillation. Notice that the vortex shedding problem is most worrisome for the low order modes. This coincides with experience in actual motor problems. One should be most concerned with the acoustic modes with the lowest frequencies, usually the longitudinal modes. Since δ is a measure of the strength of the shear stresses, it is obvious that one should seek to design grain configurations that promote smooth gas flow (large δ) without abrupt changes in contour and without the forcing of large mass flow into constricted channels. This effect was demonstrated in a series of static test firings of operational motors[2] utilizing grain modifications aimed at aerodynamic refinement of the internal flow. Smoothing of the transition region from the forward slots to the centerbore and removal of the constricting "doughnut" totally eliminated the vortex driven oscillations.

Conclusions

A comprehensive theory for vortex generated sound in solid propellant rocket motors has been demonstrated. As expected (on the basis of experimental evidence from many sources), the dipole sound source mechanism dominates.

Presence of highly-sheared flow is not alone sufficient for significant driving of waves. In fact, the presence of large-scale structures can be felt in the chamber as damping under some condition. A downstream impingement surface must be present in the proper location and orientation relative to vortex structures produced by hydrodynamic instability to produce dipole vortex driving. Interaction of the acoustic waves with the sensitive flow at the shear layer origin has been shown to set the vortex amplitude and phase relative to the acoustic field. This is an explicit model for the "feedback" phenomenon which is clearly evident in many decades of experimentation. It is based entirely upon a rational model of the fluid mechanics of the problem and does not require introduction of ad hoc assumptions regarding possible "hydrodynamic" feedback or acoustic reflections from impingement surfaces. The well-known sensitivity to the geometry of the shear layer/impingement surface system is shown to result from phasing of the hydrodynamic force on the surface relative to the acoustic wave structure and not on a feedback signal of obscure origin.

Acknowledgment

This work was supported by the Chemical Systems Division of the United Technologies under Air Force Contract FO4611-83-C-0003.

References

[1]Dunlap, R., Blackner, A. M., Brown, R. S., and Waugh, R. C., "Internal Flowfield Studies in a Simulated Longitudinally-Slotted Rocket Chamber," Paper presented at 22nd JANNAF Combustion Conference, CPIA Pub. 432, Vol. II, Oct. 1985, Pasadena, CA, pp. 163-176.

[2]Dawson, M. C., Dawson, M. C., Andrepont, W. C., Luther, D. R., and Flandro, G. A., "Elimination of Flow Induced Instabilities in Solid Rocket Motors by the Aerodynamic Contouring of Internal Grain Geometries," CPIA Publication No. 347, Vol. 1, pp. 9-21.

[3]Flandro, G. A. and Jacobs, H. R., "Vortex Generated Sound in Cavities," *Aeroacoustics: Jet and Combustion Noise, Progress in Astronautics and Aeronautics,* Vol. 37, MIT Press, 1975, pp. 521-533.

[4]Lighthill, M. J., "On Sound Generated Aerodynamically," Proceedings of the Royal Society, Series, A, Vol. 211, 1952, pp.

[5]Rockwell, D., "Oscillations of Impinging Shear Layers," *AIAA Journal,* Vol. 21, May 1983, pp. 645-664.

[6]Curle, N., "The Influence of Solid Boundaries upon Aerodynamic Sound," *Proceedings of the Royal Society,* Series A, Vol. 231, 1955, pp.

[7]Karamcheti, K., et. al., "Some Features of and Edge-Tone Flow Field," *Basic Aerodynamic Noise Research,* NASA SP207, 1969.

[8]Koopmann, G. H., "The Vortex Wakes of Vibrating Cylinders at Low Reynolds Numbers," *Journal of Fluid Mechanics,* Vol. 28, 1967, pp.

[9]Flandro, G. A., "Energy Balance Analysis of Nonlinear Combustion Instability," *Journal of Propulsion and Power,* Vol. 1, May 1985. pp. 210-221.

[10]Flandro, G. A., and Finlayson, P. A., "Nonlinear Interactions between Vortices and Acoustic Waves in a Rocket Combustion Chamber," CPIA Pub. 412, Vol. 1, Oct. 1984, pp. 71-81.

[11]Michalke, A., "On Spatially Growing Disturbances in an Inviscid Shear Layer," *Journal of Fluid Mechanics,* Vol. 23, (3), 1965, pp. 521-544.

[12]Freymuth, P., "On Transition in a Separated Laminar Boundary Layer," *Journal of Fluid Mechanics,* Vol. 25, 1966, pp. 683-704.

[13]Culick, F. E. C., "Rotational Axisymmetric Mean Flow and Damping of Acoustic Waves in a Solid Propellant Rocket," *AIAA Journal,* Vol. 4, Aug. 1966, pp. 1462-1464.

[14]Dunlap, R. and Brown, R. S., "Exploratory Experiments on Acoustic Oscillations Driven by Periodic Vortex Shedding," *AIAA Journal,* Vol. 19, March 1981, pp. 408-409.